Acta Oceanol. Sin., 2023, Vol. 42, No. 7, P. 124–137
https://doi.org/10.1007/s13131-023-2161-2
http://www.aosocean.com
E-mail: ocean2@hyxb.org.cn

Experimental study on the mitigation effect of mangroves during tsunami wave propagation

Cheng Chen[1]*, Chen Peng[1], Hui Yan[1], Minjian Wei[1], Tingyu Wang[1]

[1] College of Civil Engineering, Fuzhou University, Fuzhou 350108, China

Received 29 August 2022; accepted 5 December 2022

Abstract

Mangroves are crucial for protecting coastal areas against extreme disasters such as tsunamis and storm surges. An experimental study was conducted to determine how mangroves can mitigate the tsunami wave propagation. The test was performed in a flume, where mangrove models were installed on a slope, and dam-burst waves were used to simulate tsunami waves. To study how mangrove forests reduce the impact of tsunamis, this paper measured the heights of the incoming waves under different initial conditions (tsunami wave intensity and initial water depth) and plant factors (arrangement and distribution density) and described the reduction process. The results show that, after passing through the mangrove, the tsunami bore height will decrease within a certain range as the initial water depth increases. However, there is no correlation between the increase of inundation level and the drop of water level. The bore height attenuation is more significant at higher density of mangroves, but after tsunami passing through the mangroves, the relative bore height will decrease. When the distribution density of mangroves is constant, the wave attenuation at different locations (before, on and after the slope) shows different relationships with the initial water depth and wave height for different models. The transmission coefficient (K_i) shows a parabolic correlation with its density. The proportion of the energy loss caused by the mangrove resistance to the total energy (E_b) is defined as C_{m2}. The variation trend of C_{m2} corresponds to the tsunami wave energy attenuation rate (C_a) and K_i.

Key words: mangroves, tsunami wave, distribution density, arrangement, transmission coefficient

Citation: Chen Cheng, Peng Chen, Yan Hui, Wei Minjian, Wang Tingyu. 2023. Experimental study on the mitigation effect of mangroves during tsunami wave propagation. Acta Oceanologica Sinica, 42(7): 124–137, doi: 10.1007/s13131-023-2161-2

1 Introduction

With broad land, abundant resources, convenient transportation and dense population, the nearshore zone has become one of the most valuable area of coastal countries for international trade and cultural exchange. However, amidst times of fierce global competition for maritime rights and interests, marine economy is also faced with many challenges (Chen et al., 2016). The extreme hydrodynamic disasters, such as tsunami and storm surge, are among the challenges. Such frequently occurred disasters threaten the personnel safety and economic development of coastal areas. A tsunami is a series of long-period surface gravity waves caused by a large and sudden displacement of water bodies in the ocean, usually the result of an earthquake, landslides or collapses below the ocean floor, a volcanic eruption, and atmospheric phenomena (Zhu et al., 2006; Wang et al., 2014). Tsunami waves generally fluctuate near the sea surface. The wave attenuation is very fast along the water depth. The tsunami wave is longer than the water depth (Thusyanthan and Madabhushi, 2008), so it is also called a shallow water wave. Pacific wide tsunamis are a rare phenomenon, occurring every 10–12 years on average (Zhao, 2011; Mao et al., 2015). Being the most common cause of tsunamis, earthquakes generate 90% of tsunamis worldwide (Mao et al., 2015). A 7.3-magnitude earthquake near the Aleutian Islands in 1946 caused tsunami in the Hawaii; the 9.5-magnitude Chilean earthquake in 2004 triggered the Indian Ocean tsunami; the magnitude 9.0 earthquake that struck off Japan's northeastern coast unleashed a savage tsunami in 2011 and the 7.4 magnitude earthquake off the coast of Indonesia in 2018 triggered a tsunami that pummeled Palu. Although tsunamis occur less frequently than storm surges do, it has caused far more casualties and economic losses than storm surges (Nistor et al., 2011).

Mangroves have well-developed roots and dense crowns. When extreme marine disasters come, their roots under the water and branches and leaves on the surface that are above the high tide level can block waves. Therefore, the effect of mangroves in energy dissipation of tsunami waves has been recognized worldwide (He, 2018). When the waves hit the mangroves, the roots and trunks of the mangroves did not deform significantly, showing a good rigidity. The gaps between its branches and leaves or roots can also enhance the turbulence, consume wave energy, and mitigate the losses and suffering associated with disasters. Therefore, mangroves are regarded as "natural coast guards".

Mangroves are rigid plants. For the experimental study of rigid plants, Zhang (1966) simulated a forest under the impact of tides in a test flume with densely and sparsely planted thick branches. The results show that when the width of the forest belt remains unchanged, the wave's attenuation is roughly the same. The trunk, branches and leaves of the forest have the same shad-

Foundation item: The National Natural Science Foundation of China under contract Nos 51809047 and U22A20585; the Fujian Provincial Natural Science Foundation under contract No. 2019J05029.
*Corresponding author, E-mail: chencheng_1117@163.com

ing coefficient, and the wave elimination effect can reach 80% to 90%. Based on the Zhujiang River Delta revetment engineering test, Huang et al. (1999) found that for the narrow-sand duplex channel, planting trees on the beach has little effect on the water level and water storage capacity of the beach, but can increase the flow rate in the main channel. Ji et al. (2008) simulated a wave-proof forest by making a model tree with rigid trunks and flexible branches. The experiment showed that the wave-proof effect would increase at wider forest belt. Harada et al. (2002) investigated the tsunami mitigation effects of different subjects, including mangroves, common trees in coastal regions, wave-absorbing stones, rockfill embankments and houses. Based on the solitary wave energy equation, Chen et al. (2017) analyzed how the wave propagation deformed after the tsunami passed through the plant model. Wang (2011) analyzed the changes of wave propagation when tsunami waves passed through mangroves based on the definition of plant density in forestry. Many scholars have explored how hydrodynamic factors and plant factors influence the plants' wave reduction effect. For example, Mazda et al. (2006) found that when the mangrove forest zone was 100 m wide, its wave reduction effect was about 20%, and this effect would be amplified in deeper water. However, the study did not consider the contribution of the forest's roots, stems and leaf crowns. Horstman et al. (2014) discovered that for nearshore plants (such as mangroves), deeper water will reduce the effect of mangrove roots. Furthermore, the wave-dissipating effect of mangroves became more apparent as the water level increased to the crown. Husrin et al. (2012) quantified the stiffness of plant roots and stems to explore the attenuation of solitary waves by mangrove forest. Based on previous studies, He et al. (2017) designed a plant model with roots, trunks, and canopies to study the interaction between nearshore plants and tsunami waves, but their plant model did not quantify the effects of the roots and leaves. Zeng et al. (2019), based on He et al. (2017), quantified the reduction effect of rigid plants on solitary waves by conceptualizing the roots, stems and leaves of the plant models.

Mangroves grow in the intertidal regions of the tropical and subtropical coastlines. Due to the large-scale development and utilization of coastal land, reclamation, aquaculture, industrial pollution and offshore oil leakage in recent decades, the area of mangroves has decreased sharply, and the trend of this reduction continues. When a tsunami disaster occurs, it is hard to observe and collect data on site. Therefore, using physical model to simulate tsunami and perform related tests is a feasible research method to study how mangroves can reduce the impact from tsunami waves. Based on the data of the Indian Ocean tsunami in 2014, Chanson (2006) used the Saint-Venant equation to analyze the waves from dam burst, and found that the analytical solution was in agreement with the observed data. The waves generated by dam burst could be used to simulate tsunami wave, and they had similar properties. In laboratory, a reservoir is used, and the water is diverted along a sluice. A sluice gate is placed to connect the reservoir with the sluice. When the sluice gate is quickly lifted, the water gushes out, forming a dam-burst wave to simulate the tsunami wave. At present, this method has been adopted by many researchers (Nouri et al., 2010; Nandasena and Tanaka, 2013; Rahman et al., 2014; Xu et al., 2021a, b).

Most scholars have studied the density distribution and pattern of mangroves, but there hasn't much research on energy dissipation by mangroves' roots, stems and crowns. This paper investigates the effect of conceptualized mangroves on simulated tsunami waves in the test flume. Section 2 describes the test flume and experimental set-up. Section 3 presents the whole process of the tsunami wave passing through the mangroves and the changes of bore height, transmission coefficient and tsunami wave energy.

2 Experimental set-up

2.1 *Facility*

The experiment was carried out in the Hydraulic Laboratory of Fuzhou University. The experimental facilities include a reservoir, a test flume, and a dam-break wave generation system (DWGS) (Figs 1a, b). The test flume consists of a sluice gate, a tsunami wave propagation flume, a slope, an adjustable water baffle and a drain channel, as shown in Fig. 1c.

The reservoir is an irregular polygon with the maximum length of 12.3 m, the maximum width of 11.5 m, a height of 0.8 m, the maximum working water depth of 0.7 m, and a storage capacity of 105 m^3. The water level in the reservoir (RWL) is dynamically maintained to a balance by adjusting an inlet valve and a drain channel. Measuring 16.5 m (length) × 1.5 m (width) × 0.8 m (height), the test flume is connected to the reservoir through a sluice gate. The sides of the water tank are made of blue bricks, with shaved concrete as its bottom, all of which are coated with waterproof asphalt to prevent leaks. The DWGS consists of a gate control box, a computer control system, and a sluice gate. The computer control system will send signals to the gate control box to quickly lift the gate.

During tsunami wave propagation, troughs may arrive first, causing the water to recede and exposing the seabed to the air. This is the dry bed condition in which the initial water level is 0. To simulate wet bed conditions, initial water depths of 0.05 m and 0.10 m were set on the flume. To be more consistent with the actual process of tsunami waves coming ashore, we use 2 m (length) ×1.5 m (width) steel plates to build 1:20 slopes in the flume. Since the width of the flume is 1.5 m and the bore height is relatively small, the flume has a large aspect ratio. Therefore, the area outside the near wall flow area is regarded as a 2D water flow, and the wall effect can be ignored.

A drain channel is set at the end of the flume. During the test, a baffle plate in front of the channel is lifted to prevent drainage and maintain water depth. After the tsunami wave hits the model, the baffle is opened to quickly drain the water out of the flume. The side wall of the flume has a glass window which enables visualization of tsunami waves.

2.2 *Generalization and arrangement of mangrove model*

The geometric similarity scale is 1:25, which has been proved to be applicable (Chen et al. 2016). The actual mangroves are 25 times larger than the model.

There are three parts of the mangrove forest that can reduce the impact of waves, the roots, the stems and leaf crowns. The stems, which are the main part of most arbor plants, will be included in all physical tests to study their effect on the waves. However, it is tricky to recreate actual plants in the lab because of the complicated geometric structures of plant roots and crowns and the density difference between roots and leaves. Therefore, some parts of the roots, stems and leaves of the plants are conceptualized in this experiment.

In practice, the roots and trunks of mangroves does not deform significantly when they were subjected to waves, showing good rigidity. Therefore, plexiglass tubes are used to make plant models. This experiment simulates the roots, stems and leaves of plants based on the size of real mangroves. The root height is 5 cm, and the acrylic cylinder with a diameter of 6 mm is used for

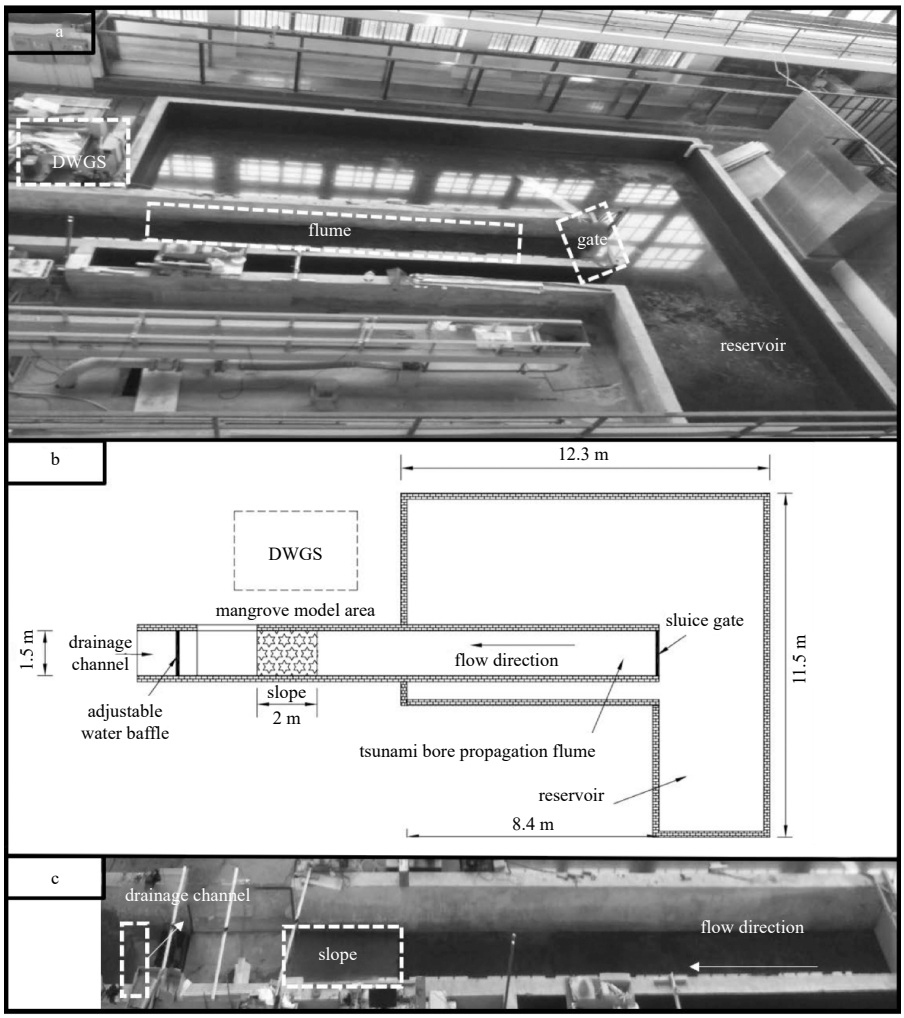

Fig. 1. Experimental facility.

simulation. Each plant consists of 16 cylinders. The stem height is 20 cm, and a cylinder with a diameter of 10 mm is used for simulation, one per plant. The leaf height is 10 cm, a cylinder with a diameter of 6 mm is used for simulation, and each plant consists of 16 cylinders. The total height of the mangrove model is 20 cm, 5 cm is just to submerge the root of the mangrove model, and 10 cm is just to reach the lower end of the leaf crown of the mangrove model. Note that the stems and leaves of the plant model are not fixed to the disc, but will oscillate with the waves within certain limits, which is in line with reality. A schematic diagram of the experimental model is shown in Fig. 2.

The mangrove model is installed on the slope of the flume. As shown in Fig. 3, a total of 6 wave gauges (WG) with a measurement range of 0–70 cm will measure the changes of tsunami bore height. In the experiment, wave gauge #1 and wave gauge #2 are placed at 1 m and 0.5 m in front of the mangrove model. Wave gauge #3 is placed at the front end of the mangrove model to measure the bore height in front of the model; wave gauge #4 is placed at the back of the mangrove model to measure the bore height behind the model; and wave gauge #5 and wave gauge #6 are located 0.5 m and 1.0 m behind the mangrove model.

As glass cement helps the placement of objects at the bottom of the flume (Fig. 4), it was used to fix the mangrove model on the slope to prevent it from being dumped by strong water currents. In practice, plants are usually arranged in a rectangular and

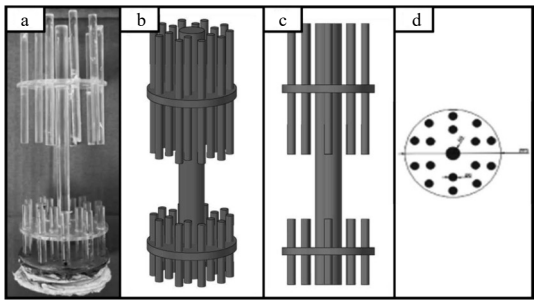

Fig. 2. Mangrove generalized model. a. Solid view; b. three-dimensional view; c. front view; d. top view.

staggered pattern. In this paper, a circular arrangement is adopted to further dissipate energy. Considering the scale of the model and the width of the flume, the model takes a square area of 0.5 m × 0.5 m. To study the effect of mangrove density on wave mitigation, models of the same arrangement but different densities are analyzed (Table 1). For example, M1, M2, M3 share the same pattern but with different density; so does the row of M4, M5, and M6; and M7, M8, and M9 at the third row. Looking vertically, we can find models M1, M4, and M7 have the same density, but different arrangement; so does the second column of M2, M5, and M8; as well as M3, M6, and M9 at the third column. This

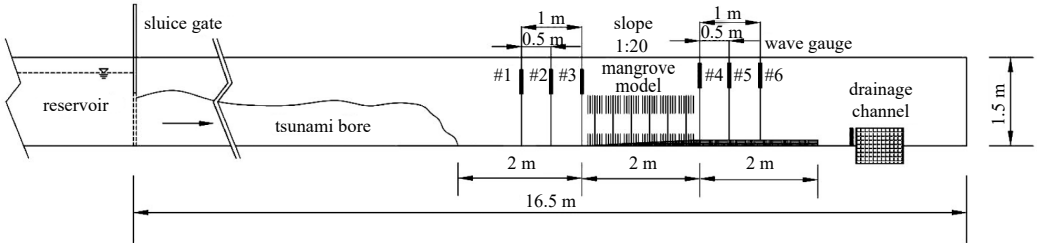

Fig. 3. Arrangement of instruments.

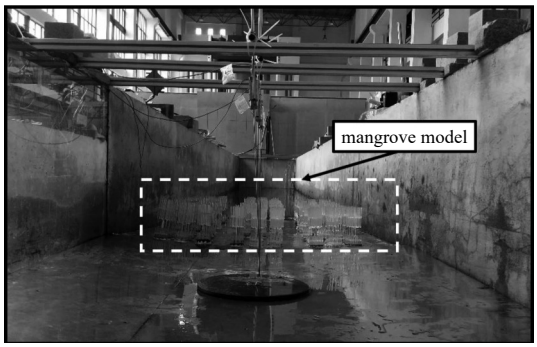

Fig. 4. The location of the mangroves in the flume.

Table 1. Experimental model parameters

Model	Arrangement	Distribution density (φ)
M1	annular	0.004 0
M2	annular	0.007 1
M3	annular	0.011 1
M4	staggered	0.004 0
M5	staggered	0.007 1
M6	staggered	0.011 1
M7	rectangular	0.004 0
M8	rectangular	0.007 1
M9	rectangular	0.011 1

is used to study the effect of arrangements on wave propagation. The distribution of model M1–M9 is shown in Fig. 5.

The arrangement of mangrove models in the test is shown in Table 1. The equation of plant distribution density in the table is given as

$$\varphi = \frac{N \times V_i}{V}, \tag{1}$$

where φ is the distribution density of mangroves; V is the volume of the entire distribution area; N represents the total number of mangroves in the distribution area; and V_i is the volume of a single mangrove model.

2.3 *Experimental conditions*

Before reaching 4 s, the tsunami bore height increases with the gate opening time, but when the time is greater than 4 s, the tsunami bore height tends to stabilize (Chen et al., 2016). After considering the experimental conditions, 5 s was taken as the gate opening time. The gate opening height (GO) and the reservoir water level are main factors to control the tsunami wave intensity. The water level in the reservoir were 0.5 m, 0.6 m, and 0.7 m. The gate opening heights were 0.25 m, 0.35 m, and 0.45 m. The initial water levels (h) of the test were 0 m, 0.05 m, and 0.10 m (Table 2). For each water depth, there were multiple combinations of reservoir water level and gate opening height. Therefore, consistent and reliable results of bore height (h_b) and bore velocity (u_b) of the tsunami under various cases were obtained.

2.4 *Data processing procedures*

2.4.1 *Bore heights*

Wave gauges were installed in the flume to measure the height and velocity the wave. When the tsunami wave passed through each gauge in turn, the time and water level was recorded by the gauge. As shown in Fig. 6, the wave reached the gauge at about 9 s, and then the water level stabilized at 10 s. When the wave passed through the gauge in the flume without model, the stable water level measured by gauge #1 was taken as the tsunami bore height (h_b), while h_i was the bore height measured under different experimental conditions. Finally, the dimensionless parameter of relative bore height was defined by h_i/h_b in the Section 3.2, and h_b/h in Section 3.3.

2.4.2 *Bore velocities*

The method of measuring the wave speed is as follows: the distance (ΔS) between two adjacent wave gauges is known, and the time interval (Δt) of the wave passing through the two adjacent gauges is recorded, then the average bore velocity between the two gauges can be calculated as $\Delta S/\Delta t$. As the bore velocity changes slightly between the gauges, the average bore velocity between two gauges can be taken as the tsunami bore velocity (u_b).

3 Results and discussion

3.1 *Reduction process of tsunami waves through mangroves*

A high-speed camera has recorded the moments of tsunami wave hitting the mangrove model, as can be shown in Fig. 7. There are six stages to describe how the tsunami wave passes through the model mangrove forests: initial impact, splash up, front-overtopping, rear-overtopping, quasi-steady overflow and recession.

At the initial impact stage, the tsunami wave, which was mixed with air to form foam, traveled to the front of the mangrove model and reached the roots. At this time, the main water body was blocked by the high-density distribution of the root system, causing the water body to splash upward, and then partially blocked by the mangrove leaf crown, and finally squeezed through the gap of the root system.

At the splash up stage, the water level rose to the mangrove canopy. At this moment, the water splashed up the front surface of the mangrove roots and leaf crowns, forming a tall water wall, the height of which could reach up to 3 times higher than the mangrove forest. As the water splashed, more air was incorporated into the water, causing the white foam to increase and move forward with the current.

At the front-overtopping stage, the splashed water began to

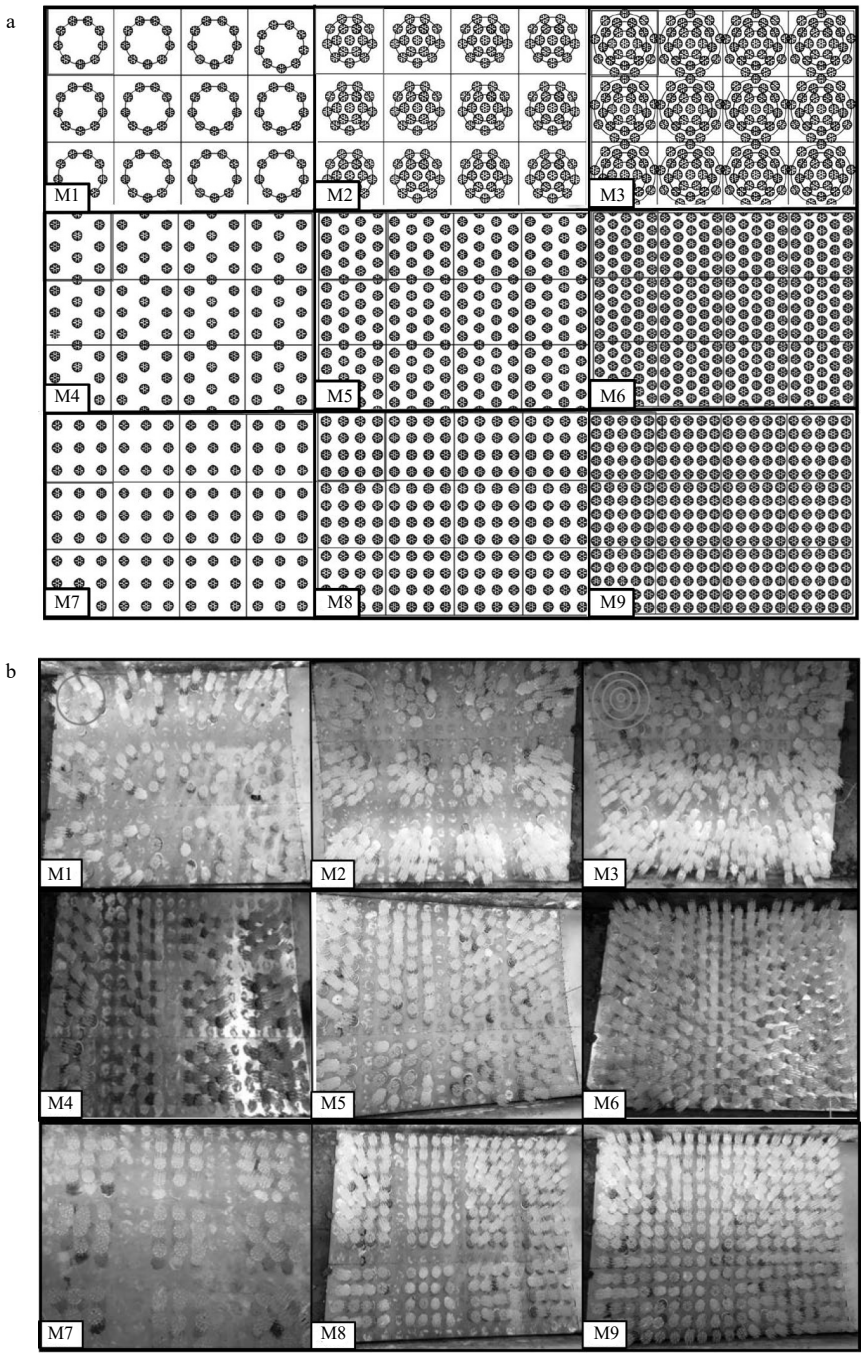

Fig. 5. Schematic diagram of mangrove model layout. a. Conceptual diagram. b. Actual diagram.

fall in the middle-part-mangroves, and the water flow began to submerge the mangroves in the front. At this time, the tsunami wave reached the leaf crown of the middle and rear mangroves.

At the rear-overtopping stage, mangrove forests located at the back are fully submerged, and white foam appeared in the arrangement area of the mangrove model. At this time, the water level in front of the slope continued to rise, and a reverse thrust was formed along the traveling direction of the tsunami wave, which offset part of the tsunami wave energy, resulting in an obvious water level height difference before and after the mangrove area.

After that, the flow converted to the quasi-steady stage, in which the white foam on the surface of the flow gradually disappeared, and the water level in the mangrove area continued to rise. The state of flow tended to be stabilized, and the water level difference between the front and rear of the mangrove model gradually shrunk.

The amount of water in the tsunami wave was limited. After the main water flow passed through the mangroves, the water level gradually dropped below the roots of the mangroves, and entered the recession stage, in which the flow velocity decreased. The recession only lasteds for 4–5 s, but when in reality, this phase will last longer.

3.2 *Variation of bore heights along flume*

3.2.1 *Bore heights for different initial water levels*

Taking the first 1 m of the mangrove model as the coordinate

Table 2. The sum of different bore heights and velocities

h/m	RWL/m	GO/m	u_b/(m·s^{-1})	h_b/m
0	0.7	0.25	3.59	0.25
	0.7	0.35	4.69	0.27
	0.7	0.45	4.99	0.28
	0.6	0.25	3.88	0.21
	0.6	0.35	3.56	0.24
	0.6	0.45	3.64	0.26
	0.5	0.25	3.48	0.19
	0.5	0.35	3.70	0.23
	0.5	0.45	3.68	0.23
0.05	0.7	0.25	3.14	0.25
	0.7	0.35	2.85	0.30
	0.7	0.45	3.02	0.33
	0.6	0.25	2.47	0.29
	0.6	0.35	2.79	0.30
	0.6	0.45	2.51	0.31
	0.5	0.25	2.41	0.25
	0.5	0.35	2.38	0.26
	0.5	0.45	2.18	0.28
0.10	0.7	0.25	2.47	0.36
	0.7	0.35	2.37	0.38
	0.7	0.45	2.37	0.38
	0.6	0.25	2.56	0.34
	0.6	0.35	2.71	0.36
	0.6	0.45	2.62	0.36
	0.5	0.25	2.24	0.31
	0.5	0.35	2.29	0.33
	0.5	0.45	2.36	0.33

origin, the wave direction can be expressed as the positive direction of the X-axis, and the Y-axis denotes (h_i/h_b) the ratio of the bore height measured by gauge (h_i) to the bore height (h_b) in the free-model case. When RWL = 0.7 m, GO = 0.35 m and the initial water level are h = 0.00 m, h = 0.05 m, and h = 0.10 m, the changes of bore height along the flume when the tsunami wave passes through the model M0–M9 can be shown in Fig. 8.

When the tsunami wave passed through the models M0–M9, the bore height increased before the slope under the three initial water levels (Fig. 8). Specifically, for h = 0.00 m, the bore height reached a maximum where no mangrove model present (X = 1 m). For h = 0.05 m and h = 0.10 m, the maximum bore height occurred at 1 m ahead of the model (X = 0 m). This is because the wave energy is sharply reduced by mangrove model, when the tsunami wave passes it. After the water flow is reflected on the slope, it superimposed with the advancing water at 1 m in front of the model (X = 0 m), resulting in a rising water level.

Comparing M1–M9 with M0, the bore height increased by 50%–120% before passing through model M1–M9, and decreased by 22%–40% afterwards. For example, the ratio of the minimum post-slope bore height to the maximum pre-slope bore height ranged from 76.53% to 79.99% for M0, while the range for M1 was 47.61% to 59.44%. The bore height reached to its minimum at the back of the mangrove model (X = 3 m), before rising at X = 3–4 m. This was caused by the flow reversal near the drain channel. As the capacity of the channel was limited, a large influx of water cannot be drained away into the channel, so the water returned.

During the experiment, the highest water level of model M1–M9 at h = 0.00 m was larger than that at h = 0.05 m and h = 0.10 m, but for h = 0.05 m and h = 0.10 m, the water level at X = 0.5 m was almost the same. This indicated that after the tsunami wave passed through the mangrove model, the bore height decreased with the increase of the initial water level within a certain range. But the decrease showed no correlation with the increase of the inundation depth.

3.2.2 *Bore heights for different wave intensities*

The intensity of the tsunami wave was determined by both RWL and GO, and the influence of the two factors on the tsunami bore height along the wave path was studied.

Figure 9 shows the variation of bore height along the wave path when the tsunami wave passes through the models M0–M9 under the conditions of h = 0.00 m, GO = 0.35 m, and three reservoir water levels (RWL = 0.5 m, RWL = 0.6 m, RWL = 0.7 m). The waves height in front of the mangrove model increased with the increase of the reservoir water level (Fig. 9). However, no matter how the reservoir water level varied, when the tsunami wave passed through the model M1–M9, the bore height curve remained parallel between X = 1 and 3 m. This indicates that the reservoir water level has no correlation with the mangrove model's effect on reducing the tsunami wave.

In Figs 9a and b, the order of relative bore heights before and after the tsunami wave passing through the model M0 were RWL = 0.7 m > RWL = 0.5 m > RWL = 0.6 m. Before passing through model M1, the tsunami wave had relative bore heights in the order of RWL = 0.7 m > RWL = 0.6 m > RWL = 0.5 m; afterwards, the order became RWL = 0.7 m > RWL = 0.5 m > RWL = 0.6 m. For the case of 70-35-0 (RWL = 0.7 m, GO = 0.35 m, h = 0.00 m), after the tsunami wave passed through the model M1–M3 (same arrangement, different density), mitigation effect followed the order of M3 > M2 > M1. It indicates that the mitigation effect of the mangrove forests was related to its distribution density. The mitigation effect of tsunami waves after it passed through models M1, M4 and M7 (same density, different arrangement) was: M1 > M4 > M7. The mitigation effect of tsunami waves in mangrove model area was related to mangrove arrangement.

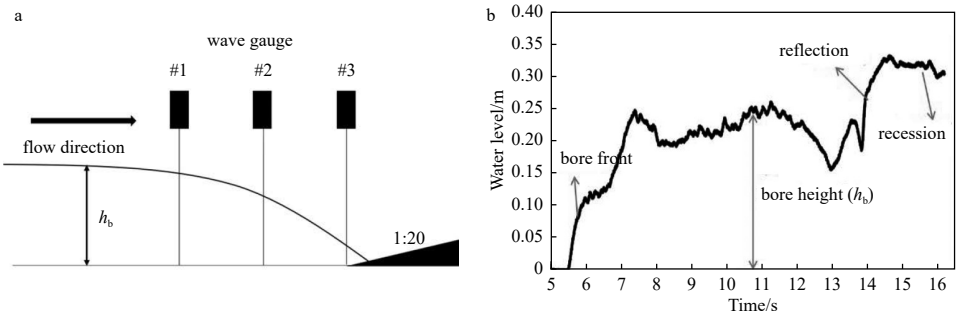

Fig. 6. Location of wave gauge and time history of water level record by wave gauge #1.

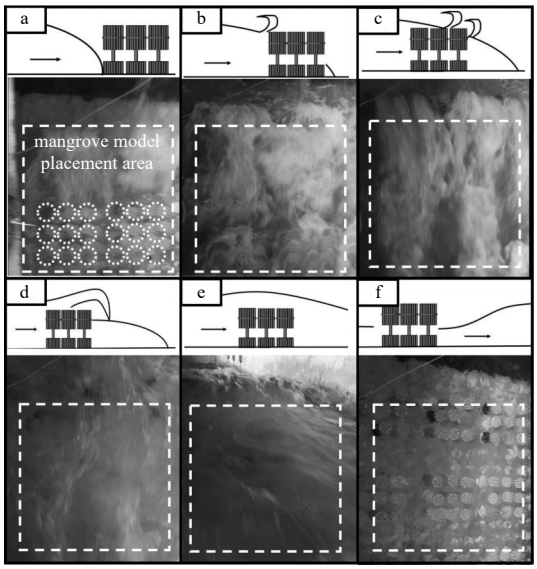

Fig. 7. The process of tsunami waves passing through the mangrove model. a. Initial impact; b. splash up; c. front-overtopping; d. rear-overtopping; e. quasi-steady overflow; f. recession.

Figure 10 shows the variation of tsunami bore height along the wave path in the no model flume. Under 3 reservoir water levels, 3 initial water level, and 3 gate opening heights, there were 27 cases in total. For h = 0.00 m and h = 0.05 m, the curves of bore heights at the three gate opening heights (GO) almost overlapped, while for h = 0.10 m, the bore height curves were slightly different, but followed the same trend. This showed that GO had little effect on the bore height, so only GO = 0.35 m would be studied in the following paper.

3.2.3 *Bore heights for different mangrove distribution densities*

Models with the same arrangement but three different distribution densities were studied to explore the effect of mangrove density on tsunami bore height (Table 1). Figure 11 shows the change of tsunami bore heights along the wave path for model M1–M9 at RWL = 0.5 m, and h = 0.00 m.

As shown in Fig. 11a, when h = 0.00 m and X = 1.0 m, the relative bore height before the tsunami wave passes through the model M0–M3 are: M3 (φ = 0.011 1) > M2 (φ = 0.007 1) > M1(φ = 0.004 0) > M0(φ = 0.000 0), and after passing through the model is M3(φ = 0.011 1) < M2(φ = 0.007 1) < M1(φ = 0.004 0) < M0(φ = 0.000 0). This indicates that the bore height is negatively correlated with the mangrove density. Figures 11b and c also demonstrate the relationship mentioned above.

Figures 11a and b shows that from model M1 to M3, the attenuation of bore height is more significant. The attenuation of tsunami bore height becomes greater with higher mangrove density, resulting in a smaller relative bore height after the model. This is because as the distribution density of mangroves increases, the contact area becomes larger. When the tsunami wave impacts the mangrove model, significant energy losses occur during the collision, resulting in greater attenuation of the tsunami bore height.

When h = 0.10 m, no matter what the arrangement density is, the bore heights are similar at the front end of the mangrove arrangement area, and grows higher after the wave passes through the back of the mangrove area (Figs 11d, f)). In other words, when X = 1.0 m, and before the tsunami wave passes through the model, bore heights are: φ = 0.000 0 ≈ φ = 0.004 0 ≈ φ = 0.007 1 ≈ φ = 0.011 1, and after the tsunami wave passes through the model, they are: φ = 0.011 1 < φ = 0.007 1 < φ = 0.004 0 < φ = 0.000 0. This indicates that the attenuation of tsunami bore height has a significant correlation with the mangrove density.

3.2.4 *Bore heights for different mangrove arrangements*

Table 1 shows that the arrangement density of models M1, M4, and M7 is 0.004 0, the arrangement density of models M2, M5, and M8 is 0.007 1, and the arrangement density of models M3, M6, and M9 is 0.011 1. Each model of the same distribution density has three different arrangements. Figure 12 shows the variations of tsunami bore heights along the wave path for models M1–M9 when RWL = 0.5 m and with three initial water levels at h = 0.00 m, h = 0.05 m, and h = 0.10 m. The effect of the arrangement of mangroves on the bore height is studied as below.

Figure 12 shows that before the tsunami passes through the mangrove model the bore heights are quite different, but after it passes through the model, they are roughly the same. Therefore, it indicates that the arrangement of mangroves has a significant effect on the attenuation of bore heights. When the tsunami wave passes through the mangrove model area, a turbulent wake vortex area will be formed behind the mangroves, which will further reduce the wave energy of the tsunami. Except for Fig. 12c, when X = 1 m, the water level of the annular arrangement is the smallest, while the staggered arrangement is the largest, which indicates that the wake vortex area behind the mangroves will change with the mangroves' arrangement, resulting in different effects of energy reduction.

Figure 13 shows the change of bore height for model M1–M9 in the case of 50-35-0. When the tsunami wave passes through the M3 model (Fig. 13), the bore height is the largest, and the attenuation degree is also the largest, which corresponds to Fig. 12, indicating that the M3 model has the best wave elimination effect in the case of RWL = 0.5 m and h = 0 m.

3.3 *Analysis of wave mitigation mechanism*

3.3.1 *Effect of relative bore heights on transmission coefficient*

The transmission coefficient (K_i) is a key index to measure the wave penetration/overtopping characteristics of the slope and mangroves, and its physical meaning is the ratio of the bore height after the slope to the unimpacted bore height before the slope (Ning et al., 2016). Its size reflects the ability of the test model to reduce waves. The smaller the K_i, the stronger the wave reduction effect and the weaker the wave permeability, and the larger the K_i means the lower energy dissipation when traversing the experimental model. The dimensionless transmission coefficients are related as (He et al., 2019a, 2019b)

$$K_i = \frac{h_a}{h_b}, \tag{2}$$

where K_i is the tsunami wave transmission coefficient, h_a is the bore height after the slope (after passing through the mangroves, the average recorded by WG #4 and WG #5, see in Fig. 14) and h_b is the unimpacted bore height before the slope (the average recorded by WG #1 and WG #2). To further study the relationship between tsunami bore height and initial water depth, the dimensionless parameter h_b/h is defined as the relative bore height.

Figure 15 shows the variation of transmission coefficient with bore height under different density distribution and arrangement of mangrove models.

In the flume without the model (M0), the transmission coeffi-

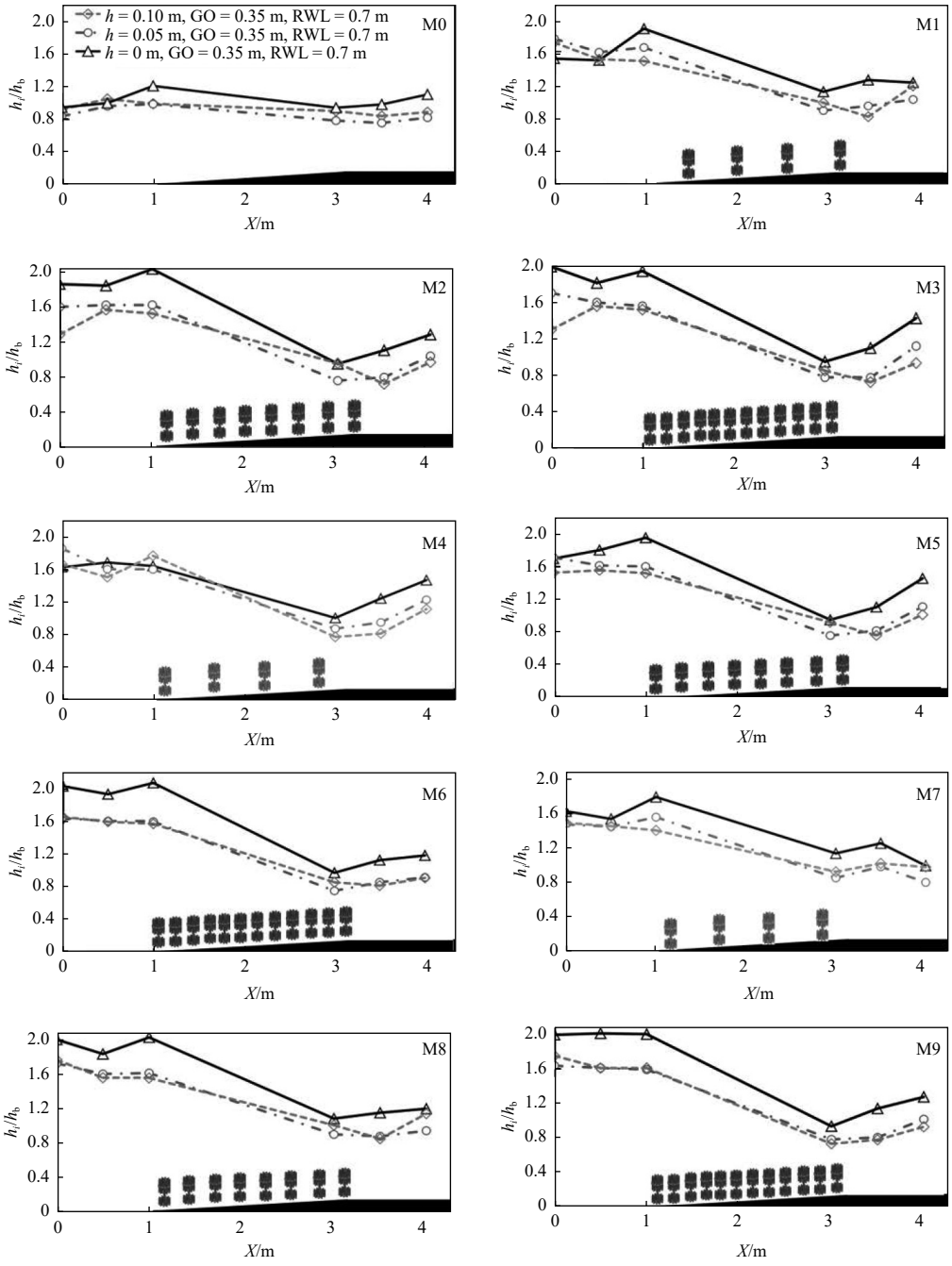

Fig. 8. Variation of tsunami bore height along the wave path under different initial water levels (h = 0.00 m, h = 0.05 m and h = 0.10 m).

cient K_i is about 0.85 after the tsunami wave lands on the slope. This indicates that the slope has a certain effect on the transmission coefficient. When the density distribution of mangroves (φ) is 0.004 0 (Fig. 15a), K_i will slightly increase with the rise of h_b/h. This indicates that, at lower density of mangrove forests, the wave attenuation will be greater as h_b/h increases, and the variation range of K_i is 0.49–0.89. For h_b/h < 15, the order of K_i is M1 > M7 > M4, so the staggered arrangement (M4) has the best wave elimination effect. For h_b/h > 15, the order of K_i is M4 > M7 > M1, so the annular arrangement (M1) has the best wave elimination effect.

For the case of φ = 0.007 1 (Fig. 15b), only the K_i of M5 decreases as h_b/h increases, and the K_i of other models remains constant with the increase of h_b/h. For annular and rectangular arrangements, the wave elimination effect of mangrove forests is not affected by h_b/h, but for staggered arrangements, the effect will increase as the h_b/h decreases. For h_b/h < 15, the rectangular arrangement (M8) can best resist bore impact. For h_b/h > 15, the staggered arrangement (M5) can best resist bore impact.

For the case of φ = 0.011 1 (Fig. 15c), only the K_i of M3 decreases with the increase of h_b/h (K_i = 0.41–0.62). K_i of other models increases with the increase of h_b/h (K_i = 0.34–0.60). For h_b/h < 20, the order of K_i is M3 > M6 > M9, and the rectangular arrangement (M9) has the best wave elimination effect. For h_b/h > 20, the order of K_i is M6 > M9 > M3, and the annular arrangement (M3) has the best wave elimination effect.

K_i in annular arrangement (Fig. 16b) decreases slightly with the increase of h_b/h, indicating that K_i is independent of h_b/h. Staggered arrangement (Fig. 16c) has K_i increases with the in-

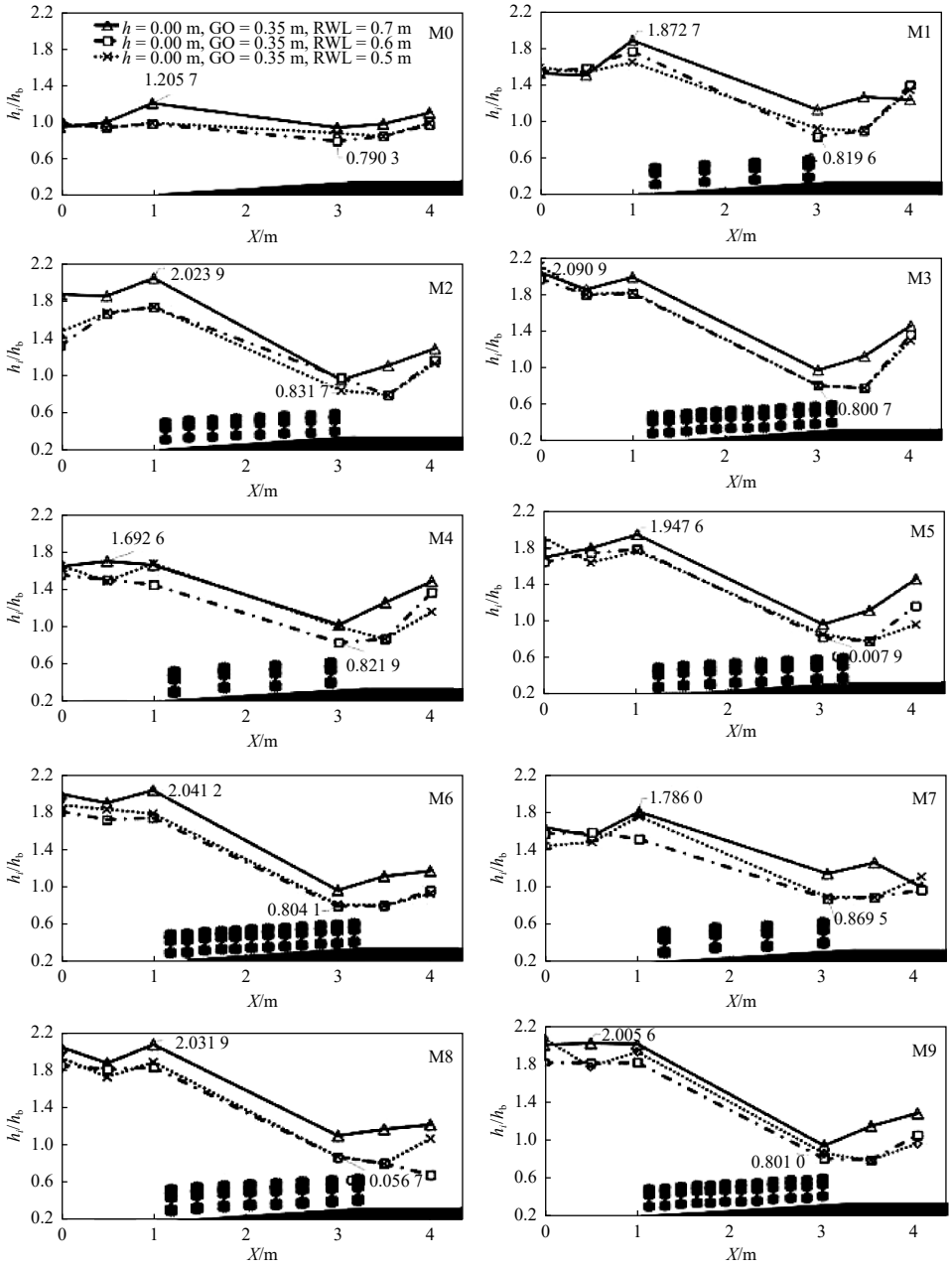

Fig. 9. Variation of bore height along the route under different reservoir water levels (RWL = 0.5 m, RWL = 0.6 m and RWL = 0.7 m).

crease of h_b/h, only for φ = 0.004 0, and K_i of other models decreases with the increase of h_b/h. Rectangular arrangement (Fig. 16d) with greater density has better wave mitigation effect. According to Fig. 16a, the order of K_i is φ = 0.011 1 < φ = 0.007 1 < φ = 0.004 0 < φ = 0.000 0, which indicates that denser mangrove models can better reduce waves regardless of the arrangement.

3.3.2 *Effect of mangrove distribution density on transmission coefficient*

Figure 17 shows the variation of the transmission coefficient with the distribution density of mangroves at different mangrove arrangements. The transmission coefficient decreases as the mangrove density increases. From φ = 0.000 0 to φ = 0.004 0, the transmission coefficient decreases rapidly in the range of 17.44%–40.48%; from φ = 0.004 0 to φ = 0.011 1, the decrease range is 2.30%–31.05%. This is because for φ = 0.000 0, the tsunami wave passes through the slope, and the wave energy is only attenuated by the slope. For φ = 0.004 0, the interaction between tsunami waves and mangroves generate turbulence, which contributes to the most energy loss of the tsunami wave. As shown in Fig. 17, the transmission coefficients of tsunami waves under different mangrove model arrangement are: staggered<annular<rectangular. Therefore, staggered pattern is most suitable for wave resistance.

3.3.3 *Energy change in mangrove arrangement area*

According to Bernoulli's principle, the energy change in the process of tsunami wave propagation can be expressed by the following equation, which is adopted by many researchers (Chen et al., 2016; Mokhtar et al., 2019),

$$p + \frac{1}{2}\rho {v_b}^2 + \rho g h_b = p + \frac{1}{2}\rho {v_a}^2 + \rho g h_a + E_{loss}, \quad (3)$$

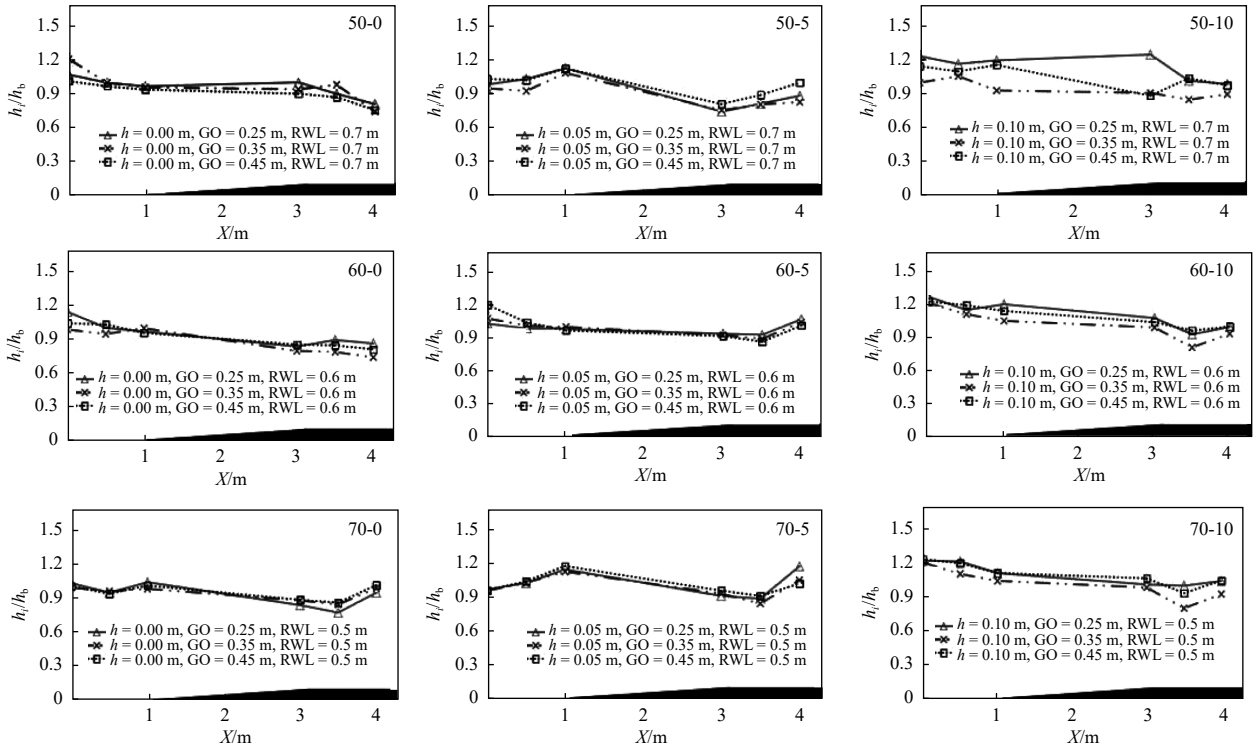

Fig. 10. Effect of different gate opening heights on tsunami bore height (GO = 0.25 m, GO = 0.35 m and GO = 0.45 m).

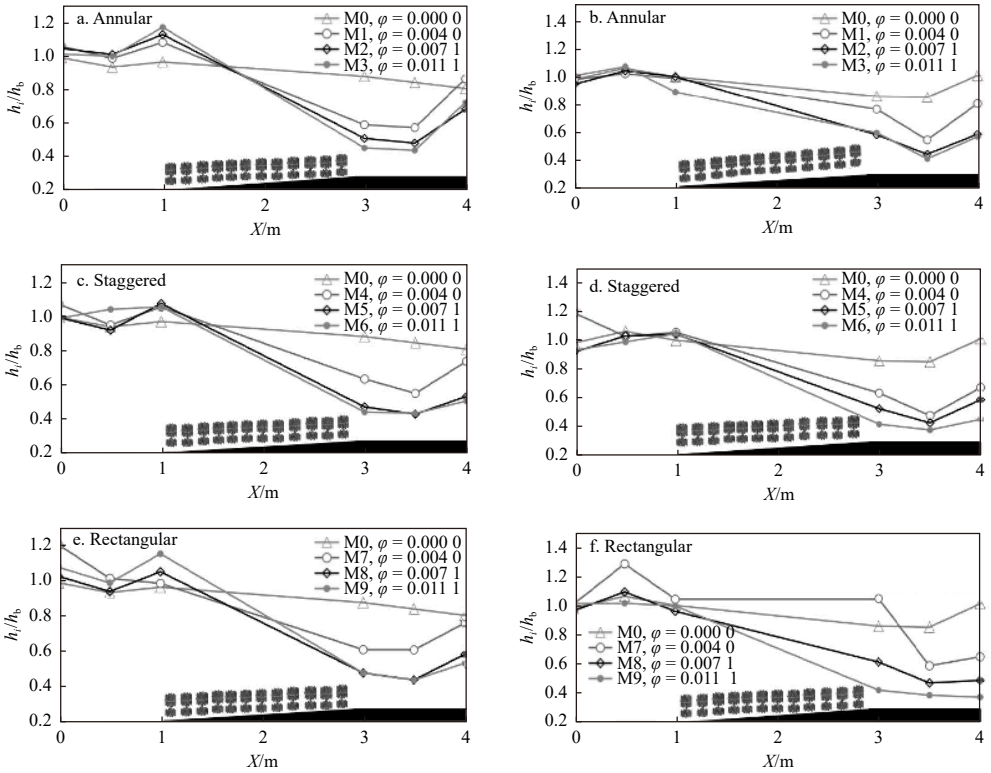

Fig. 11. Variation of bore height along the route under different mangrove distribution densities for h = 0 m (a, c, e) and h = 0.10 m (b, d, f).

where p is atmospheric pressure, in this study as 0, ρ is the water density (10^3 kg/m^3), g is the acceleration of gravity (9.81 m/s^2), v_b is the bore velocity behind of the tsunami wave propagation direction and v_a is the bore velocity ahead, E_{loss} is the energy loss of the tsunami wave from h_b to h_a (Fig. 18a).

In this study, waves were weakened by depth-induced wave breaking and mangrove resistance. The energy loss in experiment M0 is the wave attenuation due to the depth-induced wave

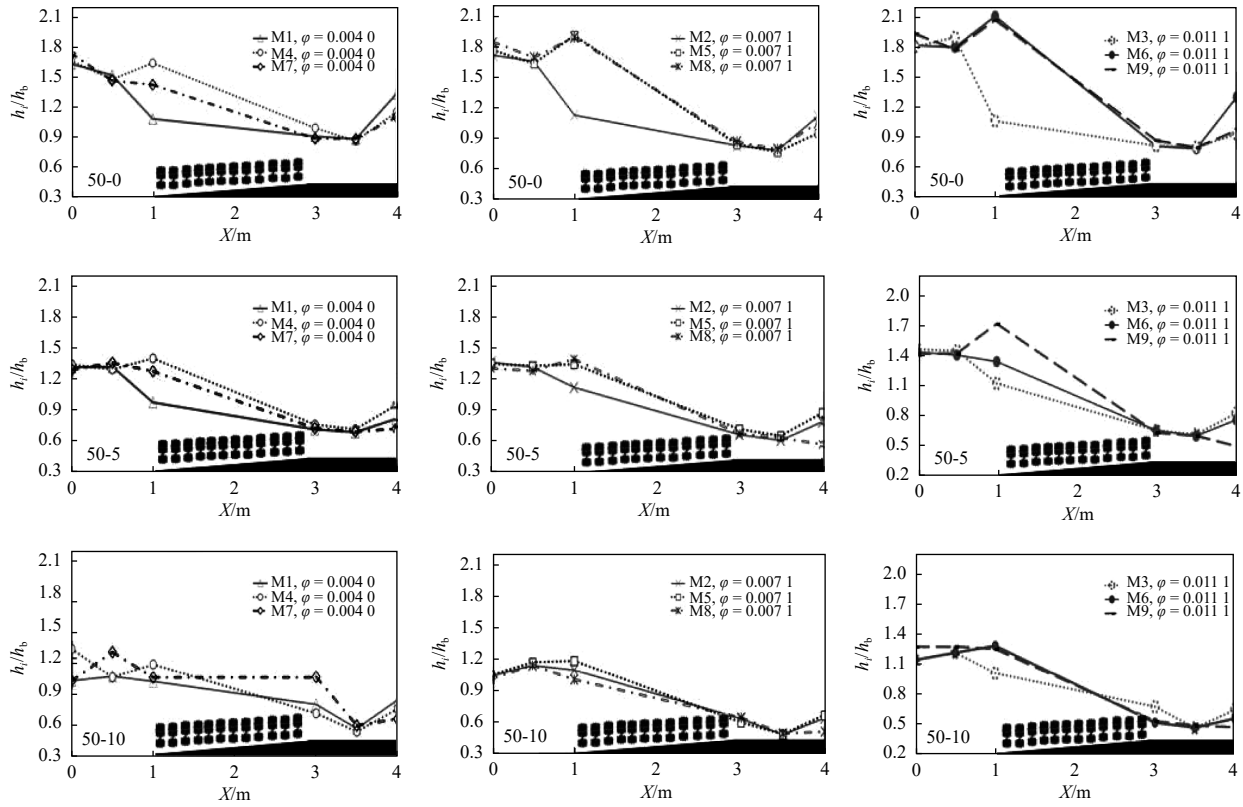

Fig. 12. Variation of tsunami bore heights along the route under different arrangements of mangroves (in the case of RWL = 0.5 m, three initial water levels and three mangrove arrangements).

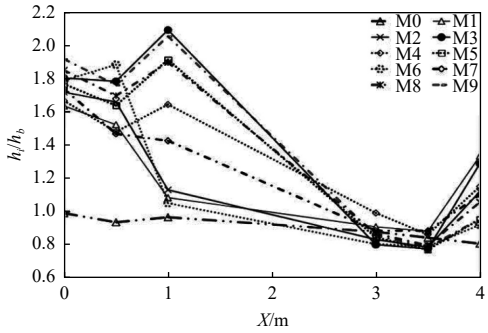

Fig. 13. Variation of bore height along the wave path in the case of 50-35-0.

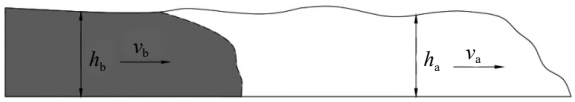

Fig. 14. Schematic diagram for Eq. (2) and Eq. (4).

damage (without mangrove resistance). When discussing the contribution of mangroves to wave attenuation, depth-induced wave breaking needs to be removed from each experimental result. Therefore, based on Bernoulli's principle, the following equation can be used,

$$\frac{1}{2}\rho {v_{\rm b}}^2 + \rho g h_{\rm b} = \frac{1}{2}\rho {v_{\rm aM0}}^2 + \rho g h_{\rm aM0} + E_{\rm d}, \tag{4}$$

where $E_{\rm d}$ is the energy loss due to the depth-induced wave breaking (Fig. 18b). Then $E_{\rm d}$ can be obtained by the following formula

$$E_{\rm d} = \frac{1}{2}\rho({v_{\rm b}}^2 - {v_{\rm aM0}}^2) + \rho g(h_{\rm b} - h_{\rm aM0}), \tag{5}$$

where $v_{\rm aM0}$ and $h_{\rm aM0}$ is the bore velocity and bore height after the slope for the case of no mangroves.

Figure 19 shows that the energy loss caused by the depth-induced wave breaking changes with the increase of the initial water depth. It can be seen from the figure that $E_{\rm d}$ decreases with the increase of the initial water depth. This is because the presence of the initial water depth reduces the energy loss of the tsunami wave due to friction at the bottom of the tank during propagation.

In the case of with mangroves, Eq. (3) can be written as

$$\frac{1}{2}\rho {v_{\rm b}}^2 + \rho g h_{\rm b} = \frac{1}{2}\rho {v_{\rm a}}^2 + \rho g h_{\rm a} + E_{\rm d} + E_{\rm m}, \tag{6}$$

where $E_{\rm m}$ is the energy loss caused by the mangrove resistance (Fig. 16c). Then $E_{\rm m}$ can be written as

$$E_{\rm m} = \frac{1}{2}\rho({v_{\rm b}}^2 - {v_{\rm a}}^2) + \rho g(h_{\rm b} - h_{\rm a}) - E_{\rm d}. \tag{7}$$

Therefore, the dimensionless parameter $C_{\rm m1}$ is defined as the proportion of energy loss caused by the mangrove resistance in the total energy loss.

$$C_{\rm m1} = \frac{E_{\rm m}}{E_{\rm m} + E_{\rm d}}. \tag{8}$$

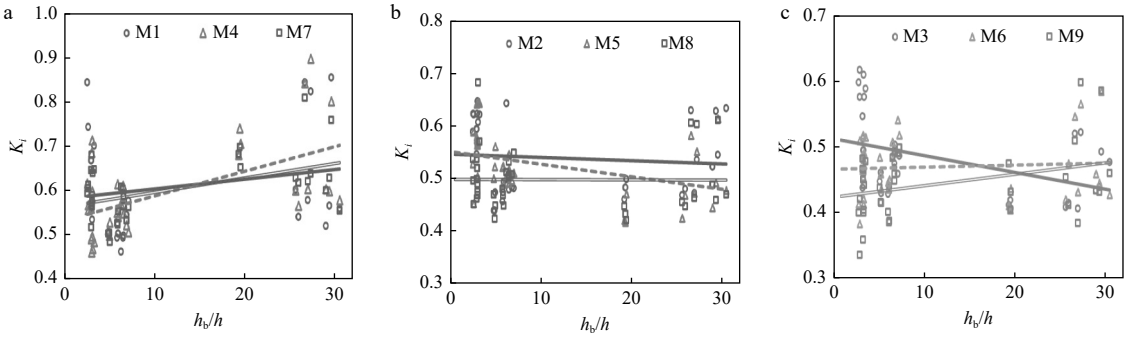

Fig. 15. Variation of transmission coefficient with relative bore height at different densities (φ = 0.004 0, φ = 0.007 1 and φ = 0.011 1).

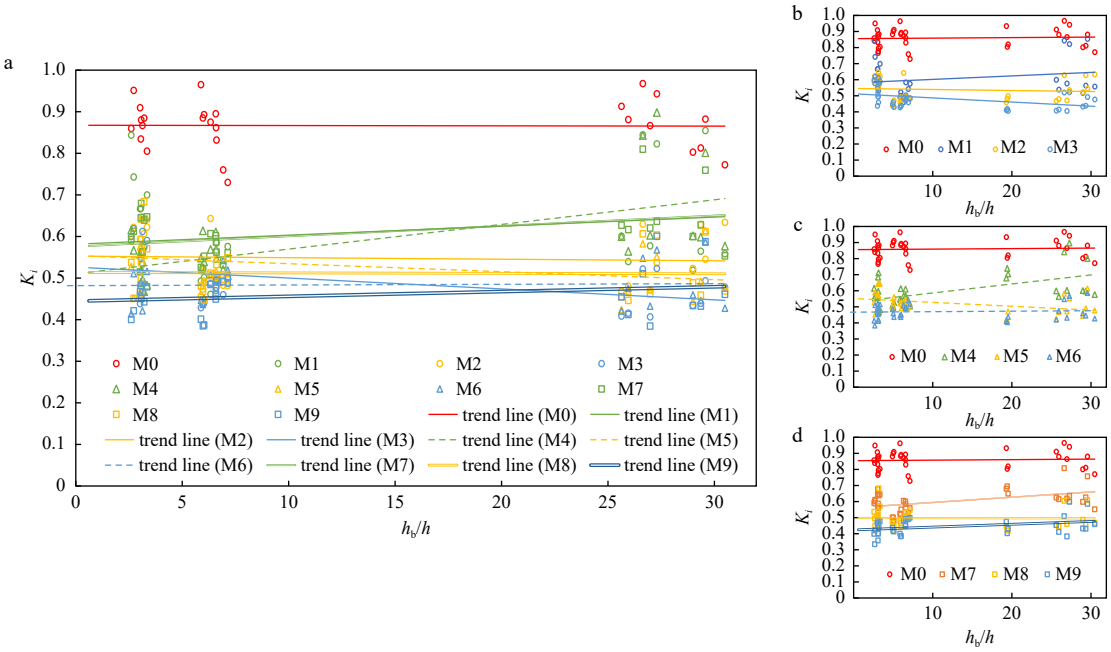

Fig. 16. Variation of transmission coefficient with relative bore height at different arrangement (annular, staggered and rectangular).

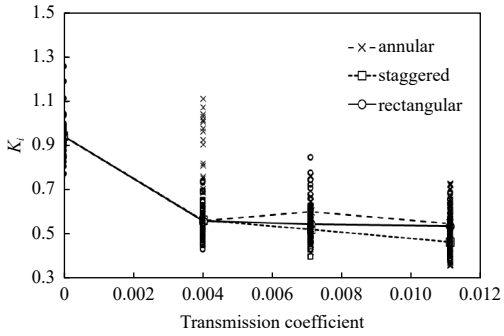

Fig. 17. Variation of transmission coefficient with the density of mangrove distribution.

It can be seen from Fig. 20 that C_{m1} increases with the increase of mangrove distribution density, but the increase is not large. In general, the C_{m1} of the three arrangements did not differ much, with C_{m1}>87.26%, which indicates that mangroves play a major role in reducing tsunami wave energy, and the reduction of mangroves increases with the distribution density of mangroves.

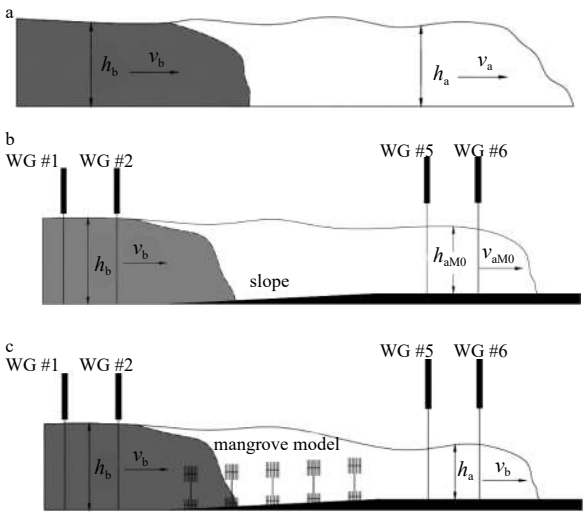

Fig. 18. Schematic diagram for Bernoulli's principle. a. Schematic for Eq. (3). b. Schematic for Eqs (4) and (5). c. Schematic for Eq. (6).

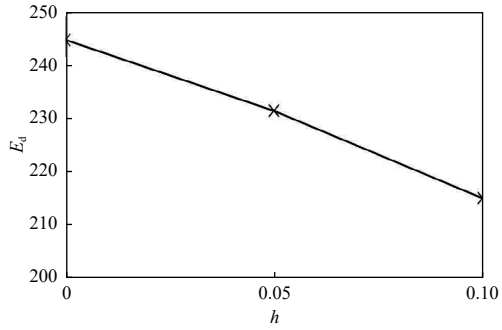

Fig. 19. Variation of E_d with the initial water level.

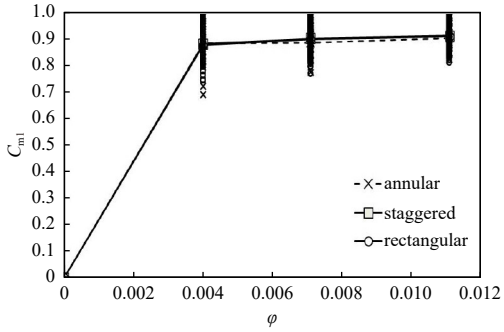

Fig. 20. Variation of C_{m1} with the distribution density of mangrove.

C_{m2} is defined as the ratio of the energy loss caused by the mangrove resistance to the total tsunami energy, and C_a is the energy attenuation rate for the tsunami wave.

$$C_{m2} = \frac{E_m}{E_b}, \tag{9}$$

$$C_a = \frac{E_a}{E_b}, \tag{10}$$

where E_b is the bore energy before the slope, $E_b = \frac{1}{2}\rho {v_b}^2 + \rho g h_b$, E_a is bore energy after the slope, $E_a = \frac{1}{2}\rho {v_a}^2 + \rho g h_a$.

Figure 21 shows that C_{m2} and C_a change with the distribution density of mangroves, respectively. It can be seen from Fig. 21a that C_{m2} increases with the increase of the distribution density of mangroves, in other words, the energy loss caused by the mangrove resistance increases in the proportion of the total tsunami wave energy. Comparing (a) and (b) in Fig. 21, it can be found that a larger C_{m2} corresponds to a smaller C_a, which also proves that mangroves account for most of the energy loss (Fig. 20, C_{m1}). Finally, it can be concluded from Fig. 21a that the staggered arrangement is the arrangement with the most wave eliminating effect, which is the same as the conclusion drawn by K_i (In Section 3.3.2, Fig. 17).

4 Conclusions

This paper studies the mitigation effect of mangrove model on the propagation of tsunami waves. The effects of initial water level (h), reservoir water level (RWL), gate opening height (GO), mangrove arrangement, mangrove distribution density (φ) and on tsunami bore height and energy were analyzed in details. The main conclusions obtained are as follows:

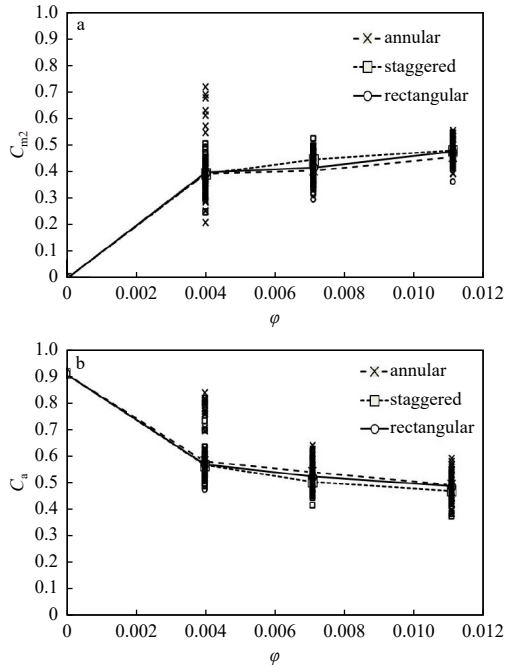

Fig. 21. Variation of C_{m2} and C_a with the distribution density of mangrove. a. Variation of C_{m2} with φ. b. Variation of C_a with φ.

(1) Compared with no mangroves, mangroves caused the bore height to rise as the tsunami wave passed through the mangrove model. The bore height increased first before passing through the mangroves and attenuated after passing through the slopes and mangrove areas and maintained the decreasing trend.

(2) The intensity of the tsunami wave is determined by both the reservoir water level and the gate opening height. The higher the reservoir level, the higher the bore height in front of the mangrove model. As the gate is lifted higher, the bore height increases until the tsunami wave reaches the slope. With the same distribution density, the relative bore heights are quite different before the tsunami passes through the mangrove model, but they are almost the same afterwards.

(3) The tsunami wave transmission coefficient (K_i) is determined by the relative bore height, the distribution density and arrangement of mangroves. The transmission coefficient decreases at higher density of mangroves.

(4) After eliminating the energy lost caused by the depth-induced wave breaking, the energy loss caused by the mangrove resistance is obtained, and the proportion of the latter to the total energy loss (E_{loss}) is defined as C_{m1}, and to the total energy (E_b) is defined as C_{m2}. The variation trend of C_{m2} corresponds to the tsunami wave energy attenuation rate (C_a), and also corresponds to the variation of K_i.

References

Chanson H. 2006. Tsunami surges on dry coastal plains: Application of dam break wave equations. Coastal Engineering Journal, 48(4): 355–370, doi: 10.1142/S0578563406001477

Chen Yurong. 2017. The new layout of marine economic development. Environmental Economy (in Chinese), (19): 24–27

Chen Cheng, Melville B W, Nandasena N A K, et al. 2016. Experimental study of uplift loads due to tsunami bore impact on a wharf model. Coastal Engineering, 117: 126–137, doi: 10.1016/j.coastaleng.2016.08.001

Chen Jie, Zhao Jing, Jiang Changbo, et al. 2017. Laboratory investigation on the effects of emergent rigid vegetation on the regular

wave transformation. Marine Science Bulletin (in Chinese), 36(2): 222–229

Harada K, Imamura F, Hiraishi T L. 2002. Experimental study on the effect in reducing tsunami by the coastal permeable structures. In: Final Proceedings of the Twelfth International Offshore and Polar Engineering Conference. Kitakyushu: The International Society of Offshore and Polar Engineers, 652–658

He Zeliang. 2018. The role of mangroves in ocean environmental protection. Environment and Development (in Chinese), 30(2): 238, 240

He Fei, Chen Jie, Jiang Changbo, et al. 2017. Experimental investigation on tsunami wave attenuation under the effects of coastal vegetation with root, stem and crown. Journal of Tropical Oceanography (in Chinese), 36(5): 9–15

He Fei, Chen Jie, Jiang Changbo. 2019a. Surface wave attenuation by vegetation with the stem, root and canopy. Coastal Engineering, 152: 103509, doi: 10.1016/j.coastaleng.2019.103509

He Fang, Zhang Huashan, Zhao Jiajun, et al. 2019b. Hydrodynamic performance of a pile-supported OWC breakwater: An analytical study. Applied Ocean Research, 88: 326–340, doi: 10.1016/j.apor.2019.03.022

Horstman E M, Dohmen-Janssen C M, Narra P M F, et al. 2014. Wave attenuation in mangroves: A quantitative approach to field observations. Coastal Engineering, 94: 47–62, doi: 10.1016/j.coastaleng.2014.08.005

Huang Bensheng, Lai Guanwen, Qiu Jing, et al. 1999. Experimental research on influence of vegetated floodplains upon flood carrying capacity of river. Journal of Hydrodynamics (in Chinese), 14(4): 468–474

Husrin S, Strusińska A, Oumeraci H. 2012. Experimental study on tsunami attenuation by mangrove forest. Earth, Planets and Space, 64(10): 973–989

Ji Hongxiang, Huang Bensheng, Qiu Xiuyun, et al. 2008. Experimental study of the influence of vegetation planting on waves deformation and wave absorbing effect. Guangdong Water Resources and Hydropower (in Chinese), (8): 14–18

Mao Xianzhong, Zhu Qian, Wei Yong. 2015. Risk analysis of potential regional earthquake tsunami on the coast of Zhejiang Province. Haiyang Xuebao (in Chinese), 37(3): 37–45

Mazda Y, Magi M, Ikeda Y, et al. 2006. Wave reduction in a mangrove forest dominated by *Sonneratia* sp. Wetlands Ecology and Management, 14(4): 365–378, doi: 10.1007/s11273-005-5388-0

Mokhtar Z A, Mohammed T A, Yusuf B, et al. 2019. Experimental investigation of tsunami bore impact pressure on a perforated seawall. Applied Ocean Research, 84: 291–301, doi: 10.1016/j.apor.2018.12.015

Nandasena N A K, Tanaka N. 2013. Boulder transport by high energy: Numerical model-fitting experimental observations. Ocean Engineering, 57: 163–179, doi: 10.1016/j.oceaneng.2012.09.012

Ning Dezhi, Zhao Xuanlie, Göteman M, et al. 2016. Hydrodynamic performance of a pile-restrained WEC-type floating breakwater: An experimental study. Renewable Energy, 95: 531–541, doi: 10.1016/j.renene.2016.04.057

Nistor I, Palermo D, Cornett A, et al. 2011. Experimental and numerical modeling of tsunami loading on structures. Coastal Engineering Proceedings, (32): 2–2

Nouri Y, Nistor I, Palermo D, et al. 2010. Experimental investigation of tsunami impact on free standing structures. Coastal Engineering Journal, 52(1): 43–70, doi: 10.1142/S0578563410002117

Rahman S, Akib S, Shirazi S M. 2014. Experimental investigation on the stability of bride girder against tsunami forces. Science China Technological Sciences, 57(10): 2028–2036, doi: 10.1007/s11431-014-5628-8

Thusyanthan N I, Madabhushi S P G. 2008. Tsunami wave loading on coastal houses: a model approach. Proceedings of the ICE-Civil Engineering, 161(2): 77–86

Wang Jun. 2011. Experimental study on interactions of tsunami wave with coastal mangrove forest. Journal of Guangdong Technical College of Water Resources and Electric Engineering (in Chinese), 9(3): 1–4

Wang Peitao, Yu Fujiang, Fan Tingting, et al. 2014. Numerical study on the linear/nonlinear characteristics and the impacts of continental shelf effects of the tsunami waves propagating. Haiyang Xuebao (in Chinese), 36(5): 18–29

Xu Zhonghou, Melville B, Nandasena N A K, et al. 2021a. Tsunami loads on slab bridges. Coastal Engineering, 165: 103853, doi: 10.1016/j.coastaleng.2021.103853

Xu Zhonghou, Melville B, Whittaker C, et al. 2021b. Mitigation of tsunami bore impact on a vertical wall behind a barrier. Coastal Engineering, 164: 103833, doi: 10.1016/j.coastaleng.2020.103833

Zeng Siyi, Chen Jie, Jiang Changbo, et al. 2019. Experimental investigation of the effects of vegetation on solitary wave attenuation based on a generalized model of root, stem and canopy. Advances in Marine Science (in Chinese), 37(4): 588–600

Zhang Jiachang. 1966. Breakwater-like wave-dissipating performance. Journal of Hydraulic Engineering (in Chinese), (2): 49–52

Zhao Xi. 2011. Numerical simulation of generation, propagation and runup of tsunamis (in Chinese) [dissertation]. Shanghai: Shanghai Jiaotong University

Zhu Huibing, Yu Ying, Dai Shiqiang. 2006. The research progress in numerical simulation of tsunami models. Journal of Hydrodynamics (in Chinese), 21(6): 714–723